Surface functionalized alumina nanoparticle filled polymeric nanocomposites with enhanced mechanical properties

Zhanhu Guo,* Tony Pereira, Oyoung Choi, Ying Wang and H. Thomas Hahn*

Received 28th February 2006, Accepted 9th June 2006
First published as an Advance Article on the web 16th June 2006
DOI: 10.1039/b603020c

Alumina nanoparticles were successfully functionalized with a bi-functional coupling agent, (3-methacryloxypropyl)trimethoxysilane (MPS), through a facile neutral solvent method. MPS was found to be covalently bound with the nanoparticles. The linked MPS was polymerized with a vinyl-ester resin monomer through a free radical polymerization. Atomic force microscope phase images showed a uniform distribution of nanoparticles. Microtensile test results revealed the Young's modulus and strength increasing with particle loading. Microscopic examinations revealed the presence of large plastic deformations at the micron scale in the nanocomposites in agreement with the observed strengthening effect of functionalized nanoparticles. Thermo-gravimetric analysis (TGA) did not show any significant change in the thermal degradation of the nanocomposite as compared with the neat resin. The polymer matrix effectively protected the alumina nanoparticles from dissolution in basic and acidic solutions.

1. Introduction

Nanomaterials have attracted much interest due to their special physicochemical properties which may be dramatically different from the bulk or atomic counterparts.[1] Synthesis of colloidal nanoparticles by the top-down (such as physical vapor deposition) or bottom-up (wet chemical) methods was subsequently explored. The reported methods to stabilize the colloidal nanoparticles—the challenge inherent with the wet chemical method—include the usage of a suitable surfactant[2–5] for long-term storage and the introduction of a noble metal shell or embedding the nanoparticles in a polymer matrix[6–8] for application in harsh environments such as acidic and basic solutions.

Nanoparticles or nanofibers have been used as fillers in both polymeric nanocomposites[9–16] to improve the mechanical, electric and optical properties, and metallic nanocomposites[17,18] to control the electrodeposition. As compared with other nanomaterials such as carbon nanotubes, alumina is cheaper and has the ability to be functionalized for nanocomposite fabrication. Vinyl ester resin was chosen due to the fact that the cured resins are thermosetting with a network structure possessing high resistance to chemicals. Upon incorporation of the alumina nanoparticles into the vinyl ester resin matrix, the obtained nanocomposite has potential applications in fabrication and building materials such as electrodeposition tank and marine vessels which require high resistance to acid or base and superior mechanical properties. The existing challenge in composite fabrication is to provide a high tensile strength due to local stress within the nanocomposite. In other words, the response of a material to an applied stress is strongly dependent on the nature of the bonds. Poor linkage between the filler and the polymer matrix such as in composites made by simple mixing[19–21] will introduce artificial defects, which consequently result in a deleterious effect on the mechanical properties of the nanocomposite.[22] However, an appropriately engineered interphase could both improve the strength and toughness of the composites, and make the nanocomposites stable in harsh environments as well.[23] The interfacial interaction between the nanoparticle and the polymer matrix plays a crucial role in determining the quality and properties of the nanocomposite, see recent reviews on the classification of organic–inorganic materials by Sanchez *et al.*[19–21] Surface functionalization of the nanoparticle with a surfactant is subsequently important not only to stabilize the nanoparticle[24] but also to render the nanoparticle compatible with the polymer.

Alumina nanoparticles[11,22,25–28] and (3-methacryloxypropyl)trimethoxysilane (MPS)[25,29–31] have been used as filler and surfactant, respectively, for nanocomposite fabrication. The functionalization of the alumina nanoparticles is normally carried out in a pH = 4 acidic alcoholic solution.[25] However, from the Pourbaix diagram,[32] alumina will get dissolved and form aluminium ions in solutions with pH values lower than 4.25 or higher than 10.25. After treatment with a normal acidic solution, the more reactive alumina nanoparticles will dissolve and reshape into agglomerated bulk form existing in the possible salt form rather than alumina any more. The other reported method used a high temperature reaction at the silane toluene refluxing point to functionalize the nanoparticles with MPS.[33]

In this paper, a facile method by using neutral MPS tetrahydrofuran (THF) solution to functionalize the alumina nanoparticles at room temperature is presented. FT-IR and TGA analytical results indicated that MPS was covalently

Multifunctional Composite Lab, Mechanical & Aerospace Engineering Department and Materials Science & Engineering Department, University of California at Los Angeles, Los Angeles, CA, 90095, USA. E-mail: zhanhu@seas.ucla.edu; hahn@seas.ucla.edu

bound onto the nanoparticle surface. The functionalized alumina nanoparticle filled vinyl ester nanocomposite showed enhanced mechanical properties under microtensile study. The fracture surface study showed an interfacial effect with the addition of the functionalized nanoparticles. The addition of the nanoparticles was observed to have no deleterious effect on the thermal stability as compared to the neat resin. The alumina nanoparticles were effectively protected from dissolution in acidic and basic solutions by embedding in the polymeric matrix.

2. Experimental

Materials

The polymeric matrix used was a vinyl ester resin, Derakane momentum 411-350 (manufactured by the Dow Chemical Company), which is a mixture of 55 wt% vinyl ester with an average molecule weight of 970 g mol^{-1} and 45 wt% styrene monomers. The liquid resin has a density of 1.045 g cm^{-3} and a viscosity of 350 centipoise (cP) at room temperature. Alumina (aluminium oxide, Al_2O_3, Nanophase Technologies) nanoparticles with an average diameter of 40 nm and a specific surface area of 44 m^2 g^{-1} were functionalized and used as a nanofiller for the nanocomposite fabrication. Trigonox 239-A (curing catalyst or initiator, organic peroxide, liquid) was purchased from Akzo Nobel Chemicals. Cobalt naphthenate (CoNap, OM Group, Inc.) was used as a catalyst promoter to decompose the catalyst at room temperature. 3-(Trimethoxysily)propyl methacrylate (MPS), tetrahydrofuran (THF, anhydrous) and ethanol (anhydrous) were purchased from Sigma-Aldrich Chemical Company. All the chemicals were used as received without further treatment.

Surface functionalization of alumina nanoparticles

In order to disperse alumina nanoparticles uniformly in the resin, MPS was used to functionalize the nanoparticles due to its bi-functional nature: hydrolysable group ($-Si(OCH_3)_3$) and unsaturated carbon–carbon double bond. The first functional group can be hydrolyzed and chemically bound to the nanoparticle surface while the latter functional group can be copolymerized with the resin monomer and form a nanocomposite. The nanoparticle functionalization is described briefly here. Alumina nanoparticles (8.545 g, 83.8 mmol) were added into a mixture of 4 g MPS and 50 ml THF. The resulting colloidal suspension was ultrasonically (Branson 1510) stirred for one hour and precipitated by sedimentation at room temperature. The precipitated nanoparticles were rinsed with THF to remove the excessive MPS and dried completely in a vacuum oven at room temperature to remove the solvent.

Nanocomposite fabrication

MPS functionalized alumina nanoparticles (specific volume percentage) were dispersed into 30 ml resin. The dispersion was carried out in an ice–water ultrasonic bath for about 1 hour. The nanoparticle/resin solution was placed into an 85 °C oven for 15 minutes under vacuum to remove gases and ensure good dispersion quality. The nanoparticle/resin solution was ultrasonically stirred in an ice–water ultrasonic bath until the temperature cooled. Then 2.0 wt% catalyst (initiator) was added into the nanoparticle/resin solution, which was stirred and degassed for 2 minutes. Promoter (0.3 wt%) was added and mixed quickly. The mixed viscous solution was poured into a ''thin-dog-bone shaped'' silicone rubber mold. The curing was performed at 85 °C for 1 hour under normal atmospheric conditions and the resulting composite was allowed to cool to room temperature naturally.

Characterization

A Fourier transform infrared (FT-IR) spectrometer was used to test the physicochemical interaction between MPS and alumina nanoparticles and the change of the MPS functional group after the nanoparticle treatment. FT-IR spectra were recorded in an FT-IR spectrometer (Jasco, FT-IR 420) in transmission mode under dried nitrogen flow (10 cubic centimeters per minute, ccpm) conditions. The liquid MPS dispersant was mixed with KBr powder, ground and compressed into a pellet. Its spectrum was recorded as a reference to be compared with that of the MPS functionalized nanoparticles.

The as-received and MPS-treated alumina nanoparticles were characterized by thermo-gravimetric analysis (TGA, PerkinElmer) from 25 °C to 600 °C with an argon flow rate of 50 ccpm and a heating rate of 5 °C min^{-1}. Thermal degradation of the nanocomposites with different nanoparticle loadings was studied by TGA.

The mechanical properties of the fabricated nanocomposites were evaluated by microtensile tests following the American Society for Testing and Materials (ASTM, 2005, standard D 1708-02a). An Instron 5544 testing machine was used to measure the tensile strength and Young's modulus. The dog-bone shaped specimens were prepared as described in the Nanocomposite fabrication section. The specimen surfaces were smoothed with an abrasive sand paper (1000) and the sanding strokes were made in the direction parallel to the long axis of the test specimen. The specimens were conditioned for more than 40 hours in an ambient environment before measurement, as required by the ASTM. Five to seven specimens per sample were tested. Specimens that broke at some obvious fortuitous flaws or near a grip were discarded. A crosshead speed of 0.15 mm min^{-1} was used and strain (mm mm^{-1}) was calculated by dividing the crosshead displacement (mm) by the gage length (mm).

An optical microscope (OM, Olympus BX41) and a scanning electron microscope (SEM, JEOL field emission scanning electron microscope, JSM-6700F) were utilized to examine the fracture surfaces. The SEM specimens were prepared by sputter coating a thin gold layer approximately 3 nm thick on a polished nanocomposite sample. The atomic force microscope (AFM, multimode, digital instruments, Veeco Company) was operated in tapping mode. AFM images were used to characterize the morphology and the functionalization of the alumina nanoparticles. Both the unpolished samples and the polished (cross-section) samples were tested to investigate the surface functionalization of alumina nanoparticles and the dispersion quality of the alumina nanoparticles within the polymeric matrix.

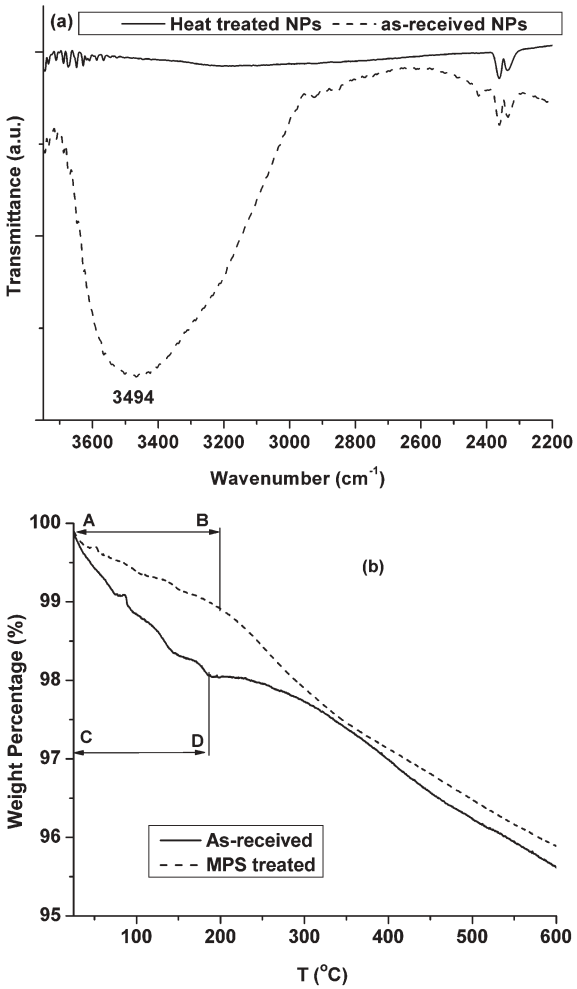

Fig. 1 (a) FT-IR spectra of the as-received and heat-treated nanoparticles; (b) TGA of the as-received nanoparticles and the MPS functionalized nanoparticles.

3. Results and discussion

Fig. 1(a) shows the FT-IR spectra of the as-received and heat-treated alumina nanoparticles. The peak at 3494 cm^{-1} in the FT-IR spectrum corresponds to the –OH stretching band indicating that the as-received nanoparticles were partially hydrolyzed. The hydrolyzed –OH disappeared after heating the as-received nanoparticles at 200 °C under vacuum condition for 13 hours. The peaks around 2376 and 2295 cm^{-1} correspond to carbon dioxide adsorbed from the atmosphere. Thermogravimetric analysis of the as-received alumina nanoparticles shows the existence of both moisture by physical adsorption and hydroxyl groups by chemical bonding in Fig. 1(b). Within the temperature range C–D, the weight loss is from evaporation of the physically adsorbed moisture. Beyond D, dehydration of chemically adsorbed water leads to weight loss as shown in Fig. 2(b).

The adsorbed moisture and the hydroxyl groups on the nanoparticle surface will react with the MPS dispersed in the tetrahydrofuran solution under ultrasonic stirring following the scheme shown in Fig. 2(a). The MPS-treated nanoparticles show less weight loss in the physically adsorbed water than the as-received nanoparticles, as shown in Fig. 1(b). The weight loss beyond point B is due to the condensation of the hydrolyzed MPS as shown in Fig. 2(c). After a TGA run, there was no color change in the as-received nanoparticles. However, the MPS-treated nanoparticles turned from white to dark grey indicating the existence and partial decomposition of the surfactant. The solubility and stability of the MPS treated alumina nanoparticles are much better in ethanol than in THF as shown in Fig. 2(d) and (e). The MPS treated alumina nanoparticles precipitated very quickly, in less than 3 hours, and the supernatant solution is very clear with a faint blue color. However, ethanol can keep the nanoparticles stable without obvious precipitation for about 5 days.

The phase contrast in atomic force microscopic phase images measured in tapping mode has been investigated for distinguishing the interphase in several systems such as E-glass fiber filled polypropylene and epoxy resin composites,[23] carbon fibers filled epoxy resin composites[34,35] and gold nanoparticle filled polymeric photoresists (PR).[36] Fig. 3(a) and (b) show the phase images of the as-received alumina nanoparticles and the alumina nanoparticles treated with MPS under AFM tapping mode. The samples were prepared by dispersing the nanoparticles in ethanol under ultrasonic stirring, dropping some of the solution on a glass slide, and evaporating the solvent naturally. The nanoparticles were observed to have different shapes, consistent with the reported TEM observation. The as-received nanoparticles and the MPS treated nanoparticles were observed to be 50.5 nm $\pm$ 16.6 nm and 59.4 nm $\pm$ 25.5 nm respectively. The AFM observed sizes are larger than the reported average size of 40 nm in both cases observed in TEM. The observed larger size in AFM than that of TEM is attributed to the convolution of the AFM tip shape and the real topography of the nanoparticles as reported for iron oxide nanoparticles.[37] Furthermore, there is a striking phase image difference between the as-received and the MPS treated alumina nanoparticles. The as-received nanoparticles were observed to have a uniform phase contrast as compared with the MPS treated alumina nanoparticles, which showed a clear polymer coating, consistent with the observed phase boundary in a gold nanoparticle filled photoresist.[36] The observed coating thickness was about 3.97 nm. This further proved that MPS was successfully chemically bound to the nanoparticle surface even after washing with ethanol.

Fig. 4 shows FT-IR spectra of the pure MPS and MPS-functionalized alumina nanoparticles. The characteristic absorption peaks at 818 cm^{-1}, 1089 cm^{-1}, and 1638 cm^{-1} are due to –Si–OCH_3, Si–O and C=C vibrations of MPS, respectively. The peaks at 1721 cm^{-1} and 1167 cm^{-1} are due to the C=O and C–O vibrations, respectively. The disappearance of the peak at 818 cm^{-1} characteristic of –Si–OCH_3 and the existence of other peaks characteristic of MPS in the MPS treated nanoparticles indicate the complete reaction between MPS and hydrolyzed alumina nanoparticles as shown in Fig. 2(a).

Abboud *et al.*[33] reported that the hydroxyl groups on the nanoparticle surface react with MPS at temperatures between 400 °C and 1100 °C. However, it was reported that

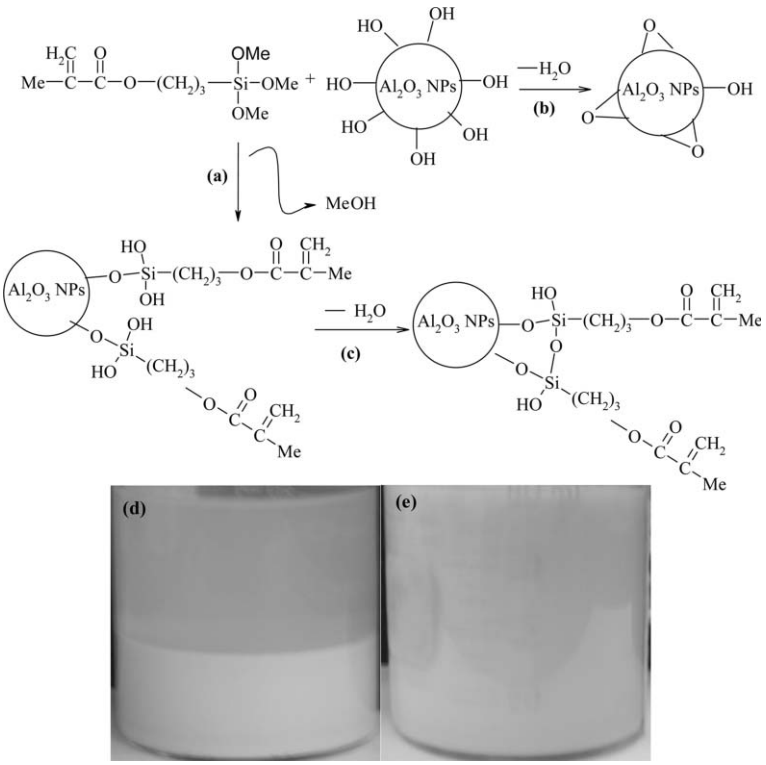

Fig. 2 Scheme of (a) alumina nanoparticle functionalization with MPS, (b) dehydration of hydrolyzed alumina nanoparticles, (c) condensation of hydrolyzed MPS, and solubility of MPS treated alumina nanoparticles in (d) THF for less than 3 hours and (e) ethanol for about 5 days.

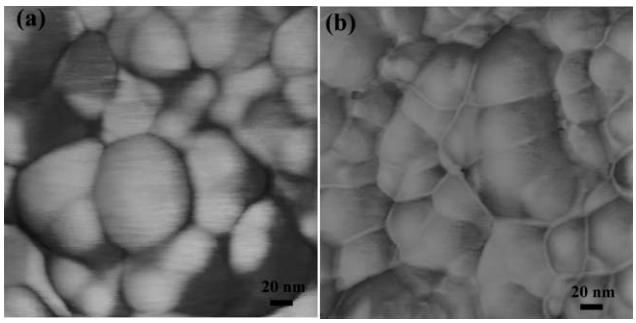

Fig. 3 Atomic force microscopy phase images of (a) as-received alumina nanoparticles and (b) MPS-treated alumina nanoparticles.

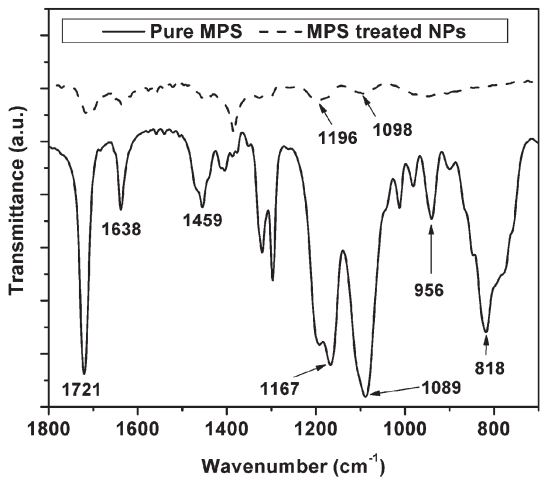

Fig. 4 FT-IR spectra of pure MPS and MPS-treated nanoparticles.

ultrasonication of a liquid caused the formation, growth and implosive collapse of bubbles, which could generate hot spots of thousands of Kelvins (~5200 K).[38–41] This method has been used in the fabrication of various nanoparticles.[39,42–46] The low-temperature nanoparticle surface functionalization reaction that happened here is from the ultrasonic stirring facilitating a local temperature increase near the nanoparticle surface.

Styrene has only one unsaturated carbon–carbon double bond and vinyl-ester monomer has two reactive vinyl end groups as shown in Chart 1. The vinyl-ester monomer provides cross-linking sites for network formation and the styrene monomer enables linear chain extension during the curing process. The cure of the resin proceeds *via* a free-radical bulk co-polymerization or homopolymerization initiated by the catalyst.

When the functionalized nanoparticles are introduced into the catalyzed vinyl-ester resin, MPS with an unsaturated carbon–carbon double bond will react with the monomers, forming a network structure. The reaction rate (0.00001 s^{-1}) of vinyl-ester resin without a promoter (cobalt naphthenate) at 95 °C reported by Li *et al.*[47] was much higher than the rate (0.0000003 s^{-1}) with the promoter at 85 °C. However, our investigation showed that the vinyl-ester resin still remained

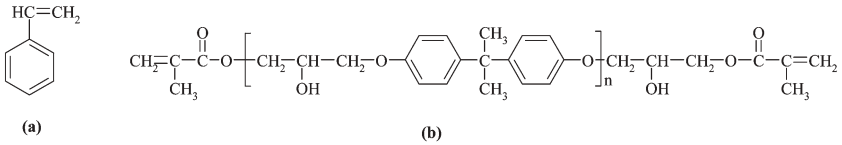

Chart 1 Chemical structures of (a) styrene and (b) vinyl-ester (VE) monomer.

liquid even after curing for 4 hours at 95 °C with the existence of the same amount of catalyst. This is possibly due to the formation of a low molecular weight polymer with a linear structure rather than a high molecular weight polymer with a network structure, indicating that the promoter was necessary for the fabrication of a high-quality solid nanocomposite. The introduction of the cobalt naphthenate promoter initiated the formation of free radicals from trigonox, which catalyzed the polymerization.

TEM, SEM and AFM have been widely used to characterize the microstructures of the nanomaterials. TEM is an optimum method to characterize 2-dimentional samples since the projected image could not locate the particle distribution within the 3-D samples; SEM and AFM are used to characterize the surface structure. Here, the particle distribution in the polymer matrix was studied with AFM by taking account of the composite surface and the cross-section of the nanocomposites after polishing. Fig. 5(a) and (b) show the typical AFM surface images of an unpolished nanocomposite with functionalized alumina nanoparticles. The nanoparticles are seen to be well dispersed with no obvious particle agglomeration. The observed phase image of a single particle as shown in the inset of Fig. 5(a) clearly demonstrates three different contrasts, which are attributed to the three different materials, *i.e.* alumina nanoparticles, MPS and the polymeric matrix. In order to study the nanoparticle dispersion quality in the interior of the nanocomposite, the sample was polished with 50 nm abrasive nanoparticles, and the AFM images(tapping mode) of the cross-section are shown in Fig. 5(c) and (d). Similar to the unpolished nanocomposite, the nanoparticles were observed to be well separated without obvious agglomeration within the nanocomposite.

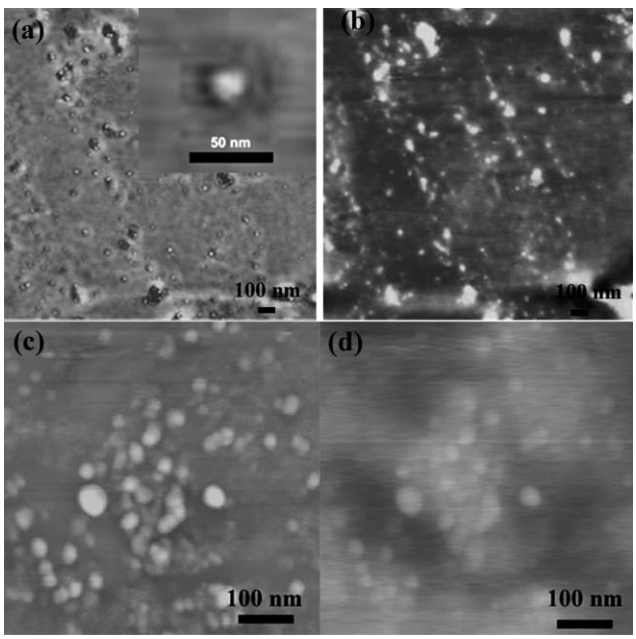

Fig. 5 Atomic force microscopy images of the cured nanocomposite with a 3 vol% functionalized alumina nanoparticle filling: (a) phase image and (b) height image of the unpolished sample; and (c) phase image and (d) height image of the cross-section of the nanocomposite after polishing (inset in (a) shows the enlargement of one nanoparticle within the matrix).

Fig. 6 shows TGA curves of nanocomposites with different particle loadings (0, 1 and 3 vol%). The TGA profile is seen to have little dependence on the presence of nanoparticles except near the high-temperature end, which arises from the different loading of alumina nanoparticles after the degradation of the polymer matrix. In other words, the addition of the alumina nanoparticles had little deleterious effect on the thermal degradation of the polymer matrix. This result is consistent with the recently reported silica-filled polystyrene nanocomposite[48] and clay filled diglycidyl ether (SC-15) epoxy nanocomposite.[49] However, it differs from the results for an unwetted alumina filled PMMA nanocomposite[26] and a silane-treated silica filled epoxy polymeric nanocomposite[50] while the latter two showed reduced thermal stability in the form of a lower glass-transition temperature.

The tensile modulus and strength of neat resin and nanocomposites were measured by microtensile tests. Fig. 7 shows typical stress–strain curves. The addition of MPS functionalized nanoparticles is seen to increase both the modulus and the strength. Also, the toughness (area under

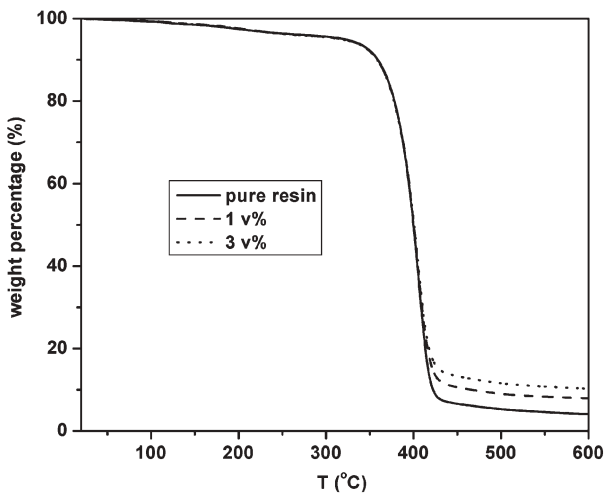

Fig. 6 Weight changes of nanocomposites with different particle loadings in TGA.

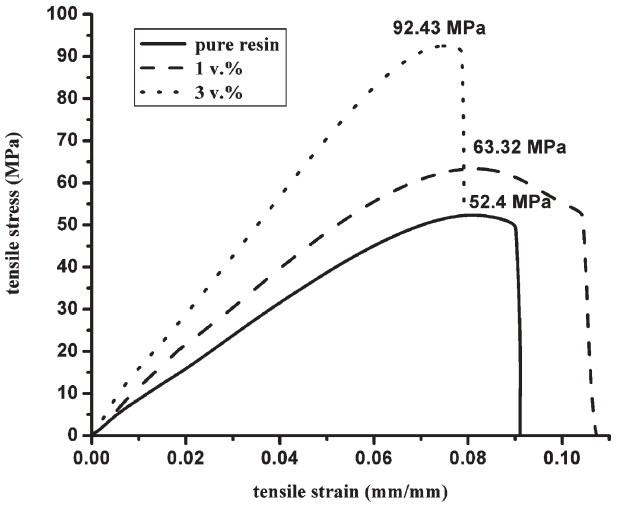

Fig. 7 Stress–strain curves of the cured pure resin, 1 vol%, and 3 vol% functionalized nanoparticle filled nanocomposites.

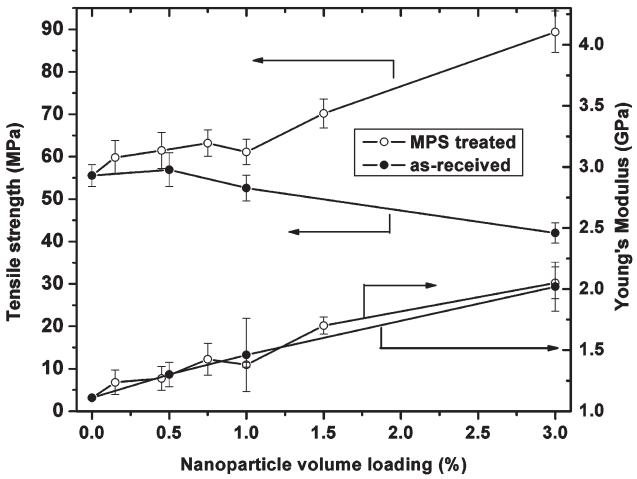

Fig. 8 Tensile strength and Young's modulus as a function of nanoparticle volume loading.

the stress–strain curve before rupture) increased significantly. Fig. 8 shows the tensile strength (the maximum stress in the stress–strain curve, MPa) and Young's modulus (the slope of the stress–strain curve in the low strain region) as a function of

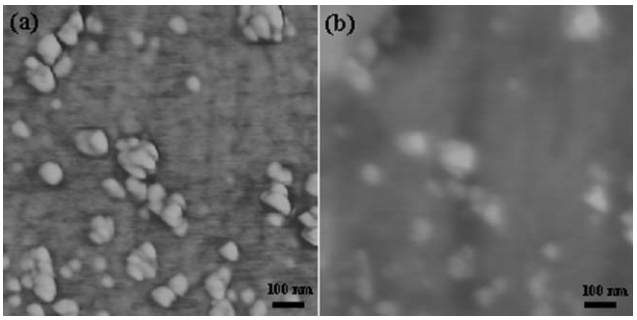

Fig. 9 Atomic force microscopy images of the cured nanocomposite with a 3 vol% as-received alumina nanoparticle filling: (a) phase image and (b) height image of the cross-section of the nanocomposite after polishing.

nanoparticle volume content. Both the tensile strength and Young's modulus increased with the increase of functionalized particle loading. Compared to the pure resin, the strength and the Young's modulus of the 3 vol% filled nanocomposite sample increased by approximately 60% and 85%, respectively. The functionalization of the nanoparticles was observed to have little effect on the Young's modulus as compared with the as-received particle filled nanocomposites. However, the reinforcing effect of functionalized nanoparticles is in stark contrast to the weakening effect of as-received particles especially at higher particle loading as shown in Fig. 8. At lower loading, the strength increased a little bit as compared with the pure resin and decreased gradually with a loading higher than 0.5 vol% as shown in Fig. 8. The strength decreased with the increase of the as-received nanoparticle loading. This can be interpreted by the particle agglomeration, the gas voids as shown in Fig. 9 (AFM image of the cross-section area of the nanocomposite after polishing) and the weak interaction between particle and polymer matrix,[19–21] consistent with the result reported for alumina-filled polyethylene nanocomposites.[22]

Both the stable thermal and enhanced mechanical properties observed here are believed to arise from the improved interfacial bonding between functionalized nanoparticles and the vinyl-ester resin. The structure between the nanoparticle and the vinyl ester resin through the coupling agent bridging is proposed in Fig. 10, which is evidenced by the AFM image with three different phases as shown in the inset of Fig. 5(a).

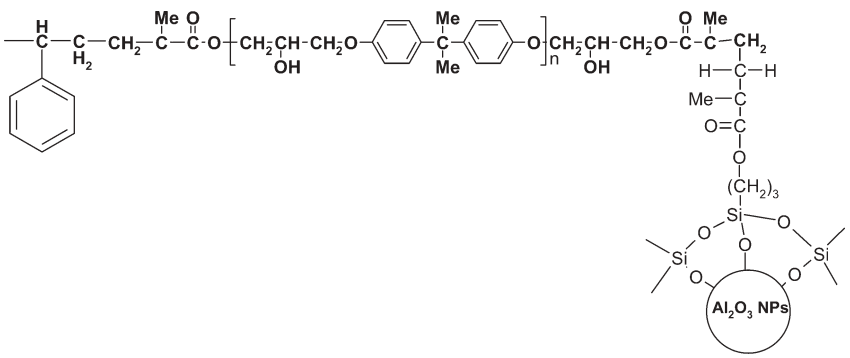

Fig. 10 Scheme of functionalized alumina nanoparticles linked with the polymer matrix.

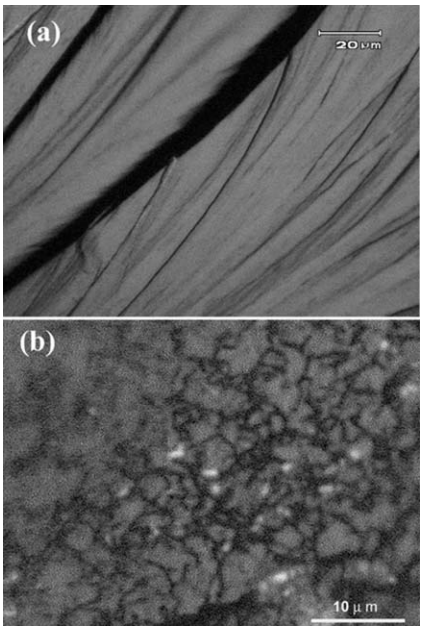

Fig. 11 Optical bright field micrographs of (a) the cured pure resin; and (b) a nanocomposite with a 3 vol% functionalized nanoparticle filling.

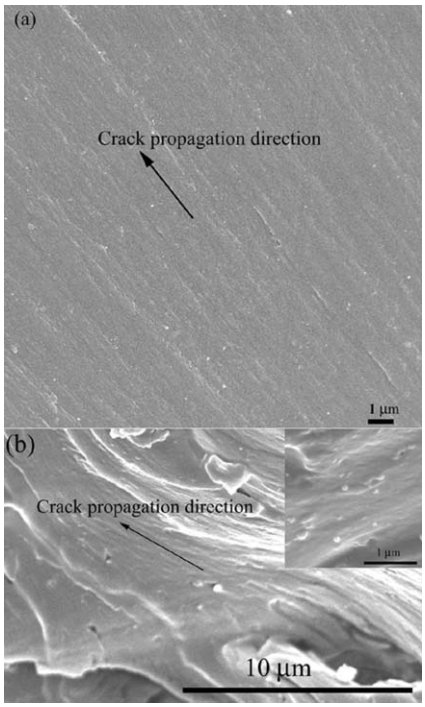

Fig. 12 SEM micrographs of (a) the cured pure resin and (b) the nanocomposite with 3 vol% functionalized nanoparticle filling (inset in (b) shows the enlarged fracture surface with nanoparticles).

The MPS serves as a chemical bond linker between the particle surface and the resin matrix. This linkage facilitates the nanocomposite behaving like a unit, in which the tough nanoparticles make the resin stronger through chemical bonding, consistent with the fact that a good interfacial interaction has a strong effect on the mechanical properties.[19] In addition, the chemical bonding between the nanoparticles and the polymeric matrix excludes air gaps, *i.e.* artificial defects between nanoparticles and the matrix, which would happen in the as-received nanoparticle filled nanocomposite seen in Fig. 9 and decrease the mechanical properties and the thermal stability.

Both the optical microscope and the scanning electron microscope were utilized to study the fracture surface of the neat resin and nanocomposite samples. Fig. 11(a) and (b) show the typical bright field optical micrographs of the fracture surface after tensile testing. The neat resin reveals brittle behavior characterized by large smooth areas, ribbons and fracture steps in the direction of crack propagation, indicating weak resistance to crack propagation. However, the nanocomposite shows a rougher fracture surface with many openings indicating increased toughness of the matrix, which originates from the secondary cracks initiated by particles at the local inhomogeneities of the primary crack front. Such a flexure surface was also reported recently in a clay-filled epoxy nanocomposite[49] and a clay filled polyamide-6 nanocomposite.[51]

Fig. 12(a) and (b) are SEM micrographs of fracture surfaces for the neat resin and 3 vol% nanocomposite. Even at the micron scale, the neat resin shows a smooth fracture surface while the nanocomposite shows a rough fracture surface. This micro-rough structure can be attributed to the matrix shear yielding or local polymer deformation between the nanoparticles rather than the intra-particle propagating cracks due to the difficulty in breaking the alumina nanoparticle arising from the high hardness[52] as compared with the resin matrix. The enlarged SEM image (the inset of Fig. 12(b)) showing the protruding nanoparticles also indicates that the cracks pass around the nanoparticle without damaging it, which was also observed in $Al_2O_3/CaSiO_3$ filled epoxy nanocomposites.[52] The protrudiong nanoparticles seen on the nanocomposite surface are observed to be covered with the matrix polymer, indicating the presence of good adhesion between the nanoparticle and the polymer matrix through the chemical bonding.[22]

In general, the presence of micron-size hard particles introduces stress concentrations, rendering the resulting composite more brittle than the matrix polymer itself. When nano-sized particles are used, however, the enhanced mechanical properties (tensile strength and Young's modulus) were observed in the case of the functionalized nanoparticle distributed uniformly within the polymer matrix. This can be explained based on the stress within the polymeric matrix, the local stress can be more easily transferred into the tougher particle with the result that the matrix appears to be amenable to a larger local plastic deformation and the end result is a higher composite strength when the particles are in intimate contact with the polymer matrix. However, the voids between the nanoparticle and the polymer matrix and the nanoparticle agglomeration result in the decrease of the tensile strength. This is justified by the reports that the physicochemical interaction between the particle and the matrix plays a significant role in the obtained composites. In other words, the strong chemical bonding improves the mechanical

properties of the composites as compared with the weak linkage by van der Waals and hydrogen bonding.[19–21] This is further consistent with the recent report on carboxylic acid and amide functionalized carbon nanotube (CNT) reinforced nylon-6 nanocomposites.[53]

In order to test the stability of the alumina nanoparticle in acidic and basic solutions, pH = 0 hydrochloric acid and pH = 14 sodium hydroxide aqueous solutions were used to treat the nanocomposites, respectively. The 3 vol% nanoparticle filled nanocomposites were immersed in de-ionized water for 24 hours for saturation, and then put into excessive acidic or basic solution for 100 hours, and finally immersed into de-ionized water again to remove the possible dissolved alumina. Alumina was predicted to be dissolved in solutions with pH lower than 4.25 or higher than 10.25 as reported in the Pourbaix diagram.[32] However, there is no observed weight change in the two cases. This indicated that the vinyl ester resin has effectively protected the alumina nanoparticle from dissolution in acidic and basic solutions. This also indicated that the nanocomposite is a solid structure which prevents the permeability or diffusion of moisture (water) into the interior of the nanocomposite.

4. Conclusion

Alumina nanoparticles have been successfully functionalized with a bi-functional silane surfactant by a facile method. With the addition of as-received nanoparticles, the vinyl ester resin nanocomposites show decreased strength due to particle agglomeration and gas voids. After nanoparticle functionalization, the formed particle/matrix interfacial bonding allows for a larger local plastic deformation in the matrix. The net result is a significant increase in both modulus and strength. The addition of the functionalized nanoparticles has no deleterious effect on the thermal stability of the composite and the vinyl ester resin after curing has effectively protected the alumina nanoparticle from dissolution in both acidic and basic solutions.

Acknowledgements

This paper is based on work supported by the Air Force Office of Scientific Research through AFOSR Grant FA9550-05-1-0138 managed by Dr B. Les Lee. The authors would like to thank Dr Ignacio Martini in the MCTP lab for his help with FT-IR spectroscopy, TGA, SEM and AFM operation. The MCTP lab is supported by the NSF IGERT Materials Creation Training Program under Grant number DGE-0114443.

References

1 I. M. L. Billas, A. Chatelain and W. A. de Heer, *Science*, 1994, **265**, 1682.
2 B. L. V. Prasad, S. I. Stoeva, C. M. Sorensen and K. J. Klabunde, *Langmuir*, 2002, **18**, 7515.
3 E. V. Shevchenko, D. V. Talapin, N. A. Kotov, S. O'Brien and C. B. Murray, *Nature*, 2006, **439**, 55.
4 P. Jeevanandam and K. J. Klabunde, *Langmuir*, 2003, **19**, 5491.
5 P. Jeevanandam and K. J. Klabunde, *Langmuir*, 2002, **18**, 5309.
6 Z. Guo, C. Kumar, L. L. Henry, E. Doomes, J. Hormes and E. J. Podlaha, *J. Electrochem. Soc.*, 2005, **152**, D1.
7 S.-J. Cho, J.-C. Idrobo, J. Olamit, K. Liu, N. D. Browning and S. M. Kauzlarich, *Chem. Mater.*, 2005, **17**, 3181.
8 Z. Guo, L. L. Henry, V. Palshin and E. J. Podlaha, *J. Mater. Chem.*, 2006, **16**, 1772.
9 V. Yong and H. T. Hahn, *Nanotechnology*, 2004, **15**, 1338.
10 J. J. Mack, L. M. Viculis, A. Ali, R. Luoh, G. Yang, H. T. Hahn, F. K. Ko and R. B. Kaner, *Adv. Mater.*, 2005, **17**, 77.
11 A. D. Pool and H. T. Hahn, *Int. SAMPE Symp. Exhib.*, 2003, **48**, 1617.
12 G. Sandi, H. Joachin, R. Kizilel, S. Seifert and K. A. Carrado, *Chem. Mater.*, 2003, **15**, 838.
13 G. Sandi, R. Kizilel, K. A. Carrado, R. Fernandez-Saavedra and N. Castagnola, *Electrochim. Acta*, 2005, **50**, 3891.
14 W. Huang and C. D. Han, *Macromolecules*, 2006, **39**, 257.
15 Y. Chen, L. Sun, O. Chiparus, I. Negulescu, V. Yachmenev and M. Warnock, *J. Polym. Environ.*, 2005, **13**, 107.
16 I. Pastoriza-santos, J. Perez-Juste, G. Kickelbkck and L. M. Liz-Marzon, *J. Nanosci. Nanotechnol.*, 2006, **6**, 453.
17 A. Panda and E. J. Podlaha, *Electrochem. Solid-State Lett.*, 2003, **6**, C149.
18 E. J. Podlaha and D. Landolt, *J. Electrochem. Soc.*, 1997, **144**, L200.
19 F. Mammeri, E. L. Bourhis, L. Rozes and C. Sanchez, *J. Mater. Chem.*, 2005, **15**, 3787.
20 C. Sanchez and F. Ribot, *New J. Chem.*, 1994, **18**, 1007.
21 P. Judeinstein and C. Sanchez, *J. Mater. Chem.*, 1996, **6**, 511.
22 X. Zhang and L. C. Simon, *Macromol. Mater. Eng.*, 2005, **290**, 573.
23 S.-L. Gao and E. Mader, *Composites*, 2002, **33A**, 559.
24 R. Shenhar, T. B. Norsten and V. M. Rotello, *Adv. Mater.*, 2005, **17**, 657.
25 D. J. Kim, P. H. Kang and Y. C. Nho, *J. Appl. Polym. Sci.*, 2004, **91**, 1898.
26 B. J. Ash, R. W. Siegel and L. S. Schadler, *J. Polym. Sci.*, 2004, **B42**, 4371.
27 K. A. DeFriend, M. R. Wiesner and A. R. Barron, *J. Membr. Sci.*, 2003, **224**, 11.
28 B. J. Ash, R. W. Siegel and L. S. Schadler, *Macromolecules*, 2004, **37**, 1358.
29 M. Zhang and R. P. Singh, *Mater. Lett.*, 2005, **58**, 408.
30 F. Bauer, H.-J. Glasel, U. Decker, H. Ernst, A. Freyer, E. Hartmann, V. Sauerland and R. Mehnert, *Prog. Org. Coat.*, 2003, **47**, 147.
31 A. P. Philipse and A. Vrij, *J. Colloid Interface Sci.*, 1989, **128**, 121.
32 M. Pourbaix, *Atlas of Electrochemical Equilibria In Aqueous Solutions*, Cebelcor, Houston, TX, 1974.
33 M. Abboud, M. Turner, E. Duguet and M. Fontanille, *J. Mater. Chem.*, 1997, **7**, 1527.
34 S.-L. Gao, E. Mader and S. F. Zhandarov, *Carbon*, 2004, **42**, 515.
35 E. Maeder, S.-L. Gao and R. Plonka, *Adv. Eng. Mater.*, 2004, **6**, 147.
36 X. Zhang, B. Sun, R. H. Friend, H. Guo, D. Nau and H. Giessen, *Nano Lett.*, 2006, **6**, 651.
37 X. Zeng, N. Koshizaki and T. Sasaki, *Appl. Phys. A*, 1999, **69**, S253.
38 K. S. Suslick, J. W. Goodale, P. F. Schubert and H. H. Wang, *J. Am. Chem. Soc.*, 1983, **105**, 5781.
39 K. S. Suslick, S. B. Choe, A. A. Cichowlas and M. W. Grinstaff, *Nature*, 1991, **353**, 414.
40 K. S. Suslick, *MRS Bull.*, 1995, **20**, 29.
41 Y. T. Didenko, W. B. McNamara, III and K. S. Suslick, *J. Am. Chem. Soc.*, 1999, **121**, 5817.
42 K. S. Suslick, T. Hyeon and M. Fang, *Chem. Mater.*, 1996, **8**, 2172.
43 H. Khalil, D. Mahajan, M. Rafailovich, M. Gelfer and K. Pandya, *Langmuir*, 2004, **20**, 6896.
44 K. Okitsu, A. Yue, S. Tanabe, H. Matsumoto and Y. Yobiko, *Langmuir*, 2001, **17**, 7717.
45 V. G. Pol, A. Gedanken and J. Calderon-Moreno, *Chem. Mater.*, 2003, **15**, 1111.

46 C.-H. Su, P.-L. Wu and C.-S. Yeh, *J. Phys. Chem. B*, 2003, **107**, 14240.
47 L. Li, X. Sun and L. J. Lee, *Polym. Eng. Sci.*, 1999, **39**, 646.
48 A. Bansal, H. Yang, C. Li, K. Cho, B. C. Benicewicz, S. K. Kumar and L. S. Schadler, *Nat. Mater.*, 2005, **4**, 693.
49 Y. Zhou, F. Pervin, M. A. Biswas, V. K. Rangari and S. Jeelani, *Mater. Lett.*, 2006, **60**, 869.
50 A. Hartwig, M. Sebald and M. Kleemeier, *Polymer*, 2005, **46**, 2029.
51 S. Wu, F. Wang, C. Ma, W. Chang, C. Kuo, H. Kuan and W. Chen, *Mater. Lett.*, 2001, **49**, 327.
52 B. Wetzel, F. Haupert and M. Q. Zhang, *Compos. Sci. Technol.*, 2003, **63**, 2055.
53 J. Gao, B. Zhao, M. E. Itkis, E. Bekyarova, H. Hu, V. Kranak, A. Hu and R. C. Haddon, *J. Am. Chem. Soc.*, 2006, **128**, 7492.

